ELSEVIER

Journal of Photochemistry and Photobiology A: Chemistry 96 (1996) 137–148

Journal of PHOTOCHEMISTRY AND PHOTOBIOLOGY A:CHEMISTRY

Absorption and fluorescence spectroscopic investigation of indocyanine green

R. Philip [a], A. Penzkofer [a,*], W. Bäumler [b], R.M. Szeimies [b], C. Abels [b]

[a] *Department of Physics, University of Regensburg, D-93040 Regensburg, Germany*

[b] *Department of Dermatology, University of Regensburg, D-93040 Regensburg, Germany*

Received 26 October 1995; accepted 1 December 1995

Abstract

Absorption spectra, fluorescence quantum distributions, fluorescence quantum yields and degrees of fluorescence polarization vs. dye concentration were determined for indocyanine green in methanol, water and aqueous albumin solution. The monomer fluorescence quantum yield is limited to a few per cent by internal conversion. In water, dimerization starts at low concentrations (approximately 3×10^{-8} mol dm^{-3}) and lowers the fluorescence quantum yield. The strong affinity of the dye to albumin shifts the onset of dimerization to higher concentrations. In methanol, dimerization is weak and closely spaced pair formation dominates at high concentrations. Dye adsorption to albumin and dye aggregation in the solvents were analysed experimentally and theoretically.

Keywords: Absorption; Fluorescence; Indocyanine green

1. Introduction

The anionic dye indocyanine green (cardio-green, ICG) [1] is widely applied in medical diagnosis [2,3] for cardiac output measurement [2,4–6], blood volume determination [7], liver function studies [8,9], pharmacokinetic analysis [10–14], choriodal angiography [15–17], object localization in tissue [18] and fluorescence probing of enzymes and proteins [19,20]. It is applied in tissue welding with near-IR light [21,22], in photosclerosis of venous varicosities [23] and photodynamic therapy studies [24].

The absorption behaviour of ICG has been studied in aqueous solution [2,25–32], saline solution [32,33], human blood plasma [2,28–30,33] and human serum albumin [28,29]. A temporal dye degradation in water [25–33], aqueous NaCl [32,33], plasma [28–30,33] and albumin [28,29] has been observed, which aggravates the accurate determination of absorption cross-sections. The dye stability in water decreases with decreasing dye concentration [29,33]. Absorption cross-section changes at elevated concentrations have been observed and attributed to dye aggregation [28–31,33]. At high dye concentrations ($C=1.3\times10^{-3}$ mol dm^{-3} [33] and $C=1.6\times10^{-3}$ mol dm^{-3} [26]) of ICG in aqueous solution [26,33] and blood plasma [26], a new J-band-like absorption band [34,35] forms within 10 days [26,33]. This indicates the slow formation of large ordered aggregates [26,33].

The fluorescence quantum yield of ICG changes when the dye is adsorbed to macromolecules such as proteins and enzymes [19,20,36]. Therefore it is applied as a fluorescent diagnostic probe in medical and biological applications [19,20,36]. Fluorescence quenching is observed in the presence of water- soluble nitro compounds [37] and hydrogen peroxide [36]. Some fluorescence quantum yield studies have been reported in Ref. [38].

In this study, the concentration-dependent absorption and emission behaviour of indocyanine green sodium iodide (ICG-NaI) in water, 50 g l^{-1} aqueous human serum albumin solution and methanol was investigated. Concentration-dependent absorption cross-section spectra, fluorescence quantum distributions, fluorescence quantum yields and degrees of fluorescence polarization were determined. The formation of dimers in water, the adsorption of ICG-NaI molecules to albumin and the closely spaced pair interaction in methanol were investigated.

2. Experimental details

The dye ICG-NaI was purchased from Pulsion, Medizintechnik, Munich [39]. The commercial name of the dye is ICG-Pulsion. Its structural formula is included in Fig. 12(b)

* Corresponding author. Tel.: +49 941 9432107; fax: +49 941 9432754.

SSDI 1010-6030(95)04292-X

(see later). The dye was used without further purification. The absorption spectrum gives no indication of dye impurity. However, the fluorescence spectrum of ICG-NaI in water excited at 632.8 nm shows a short-wavelength impurity fluorescence peak at 690 nm, probably due to a dicarbocyanine analogue to the tricarbocyanine dye ICG-NaI. The fluorescence signal of the impurity is approximately 10% of the fluorescence signal of the dye ICG-NaI. The impurity content is calculated to be less than 1%, assuming a fluorescence quantum yield more than a factor of ten higher for the impurity.

Human serum albumin [40] was purchased from Sigma (Fraction V powder, 96%–99% albumin). Its average molar mass is 69 000 g mol^{-1}. The particle mass is $m \approx 1.1 \times 10^{-19}$ g. The particles have a prolate rotational ellipsoidal shape of $a = 3.8$ nm (short axis length) and $b = 15$ nm (long axis length). The specific surface [41] is estimated to be $S \approx \pi ab/m \approx 1500$ m^2 g^{-1}. Albumin was dissolved in pH 7.4 buffer solution (Hydrion dry from Aldrich, dissolved in bidistilled water). The albumin concentration was fixed to 50 g dm^{-3}. For the aqueous solution studies, bidistilled water was used, and for the methanolic solution studies, analytical grade methanol was used without further purification.

The absorption measurements were carried out with a Beckmann ACTA M IV spectrophotometer. The sample cell thickness was adjusted to the optical density of the dye. Cell thicknesses down to 5 μm were used for the highest dye concentrations investigated (3×10^{-2} mol dm^{-3}).

The fluorescence measurements were carried out with a self-assembled fluorometer [42]. The front-face fluorescence collection technique was applied. This technique minimizes fluorescence reabsorption effects and allows fluorescence studies at high dye concentrations to be carried out. A linearly polarized 5 mW cw diode laser at 678 nm was used as excitation source. A silicon diode array system (Tracor DARRS) recorded the fluorescence spectra. The spectral sensitivity of the detection system was calibrated with a halogen tungsten lamp (Osram type HLX64625) of known colour temperature (3450 K at 12 V voltage) [43]. Absolute fluorescence quantum distributions ($E(\lambda)$) and fluorescence quantum yields ($\phi_F = \int_{em} E(\lambda) d\lambda$) were obtained using the reference dye 1,1',3,3,3',3'-hexamethylindotricarbocyanine iodide (HITCI) [44] in methanol, which has a fluorescence quantum yield of $\phi_R = 0.12$ [45]. The fluorescence quantum distributions and fluorescence quantum yields were determined under magic angle polarization arrangement [42,46] (vertically polarized excitation light in the fluorescence path, polarizer at an angle of 54.7° to the polarization of the excitation light) to avoid electric dipole reorientation effects. The degree of fluorescence polarization [47] ($P = (S_{\parallel} - S_{\perp})/(S_{\parallel} + S_{\perp})$) was determined by measuring the fluorescence signal ($S_{\parallel}$) polarized parallel to the excitation light and the fluorescence signal ($S_{\perp}$) polarized perpendicular to the excitation light. The P_F data were normalized to P_F(HITCI/methanol) = 0.16 (see below), since an accurate determination of the absolute $S_{\parallel}$ and $S_{\perp}$ values was difficult.

3. Results

In Figs. 1–3, the absorption cross-section spectra for various dye concentrations in water (Fig. 1), methanol (Fig. 2) and aqueous albumin (Fig. 3) are shown. The full curves represent the lowest dye concentrations. The absorption peaks are at $\lambda_M = 780$ nm (water), $\lambda_M = 782$ nm (methanol) and $\lambda_M = 800$ nm (albumin solution). With increasing dye concentration, the spectra change because of dye–dye interactions.

In aqueous solution (Fig. 1(a)), up to a concentration of $C \approx 10^{-4}$ mol dm^{-3}, the spectra indicate dimer formation [48–50]. The absorption spectra above $C \approx 10^{-4}$ mol dm^{-3} indicate higher oligomer formation with increasing concentration.

In methanol (Fig. 2(a)), the absorption spectrum is determined by monomers up to high concentrations ($C \leqslant 2 \times 10^{-3}$ mol dm^{-3}). The dye–solvent affinity seems to prevent dimer formation. At concentrations above $C \gtrsim 5 \times 10^{-3}$ mol dm^{-3}, the absorption spectra are modified by dye–dye interactions in statistically formed closely spaced pairs [49,50]. The average dye–dye distance is only $d = 7.7$ nm at $C = 5 \times 10^{-3}$ mol dm^{-3} ($d = (0.74CN_A)^{-1/3}$; 0.74 is the fill factor of hexagonal-close-packed spheres).

In albumin solution (Fig. 3), the monomer absorption remains practically unchanged up to a concentration of $C \approx 10^{-5}$ mol dm^{-3}. The dye molecules are preferentially adsorbed to albumin. For curve 3, the dye number density is nearly the same as the albumin number density. The albumin concentration is $C_A = 7.3 \times 10^{-4}$ mol dm^{-3}. At high dye

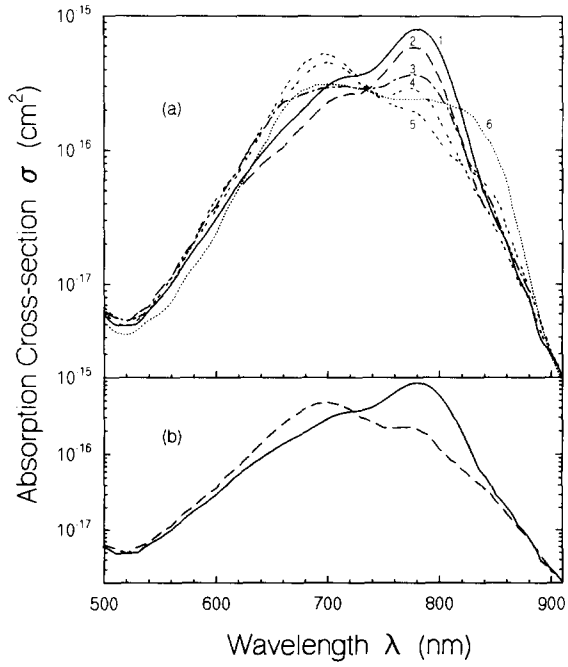

Fig. 1. (a) Concentration-dependent absorption cross-section spectra σ of ICG-NaI in distilled water. Dye concentrations (mol dm^{-3}): 1, 1×10^{-7}; 2, 1.13×10^{-6}; 3, 1.42×10^{-5}; 4, 8.5×10^{-5}; 5, 2.5×10^{-3}; 6, 1.1×10^{-2}. (b) Extracted monomer (full curve) and dimer (broken curve) absorption cross-section spectra of ICG-NaI in water (see text).

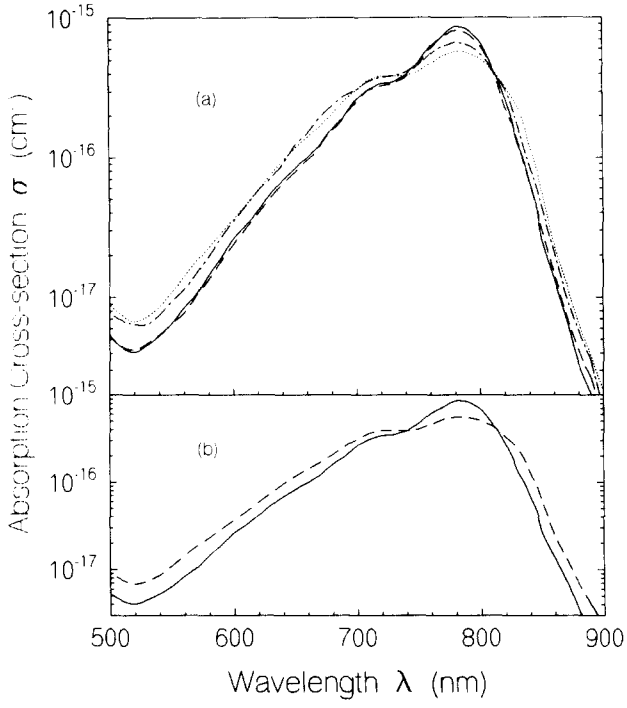

Fig. 2. (a) Concentration- dependent absorption cross-section spectra of ICG-NaI in methanol. Dye concentrations (mol dm^{-3}): full curve, 8.4×10^{-6}; broken curve, 4.2×10^{-3}; broken-dotted curve, 8.4×10^{-3}; dotted curve, 3.3×10^{-2}. (b) Extracted monomer (full curve) and closely spaced pair (broken curve) absorption cross-section spectra of ICG-NaI in methanol.

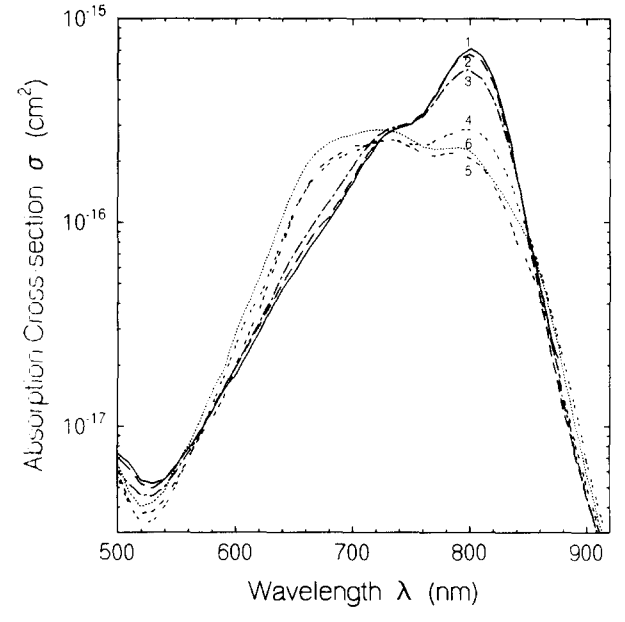

Fig. 3. Concentration- dependent absorption cross-section spectra of ICG-NaI in 50 g dm^{-3} aqueous albumin solution. Dye concentrations (mol dm^{-3}): 1, 6.7×10^{-6}; 2, 8.4×10^{-5}; 3, 8.4×10^{-4}; 4, 2×10^{-3}; 5, 8.4×10^{-3}; 6, 1.7×10^{-2}. Curve 1 represents the absorption cross-section spectrum of single ICG-NaI molecules adsorbed to albumin macromolecules.

concentrations ($C\gtrsim2\times10^{-3}$ mol dm^{-3}), the spectra indicate the presence of higher oligomers.

The fluorescence quantum distributions ($E(\lambda)$) at various dye concentrations are displayed in Figs. 4–6 for ICG-NaI in water (Fig. 4), methanol (Fig. 5) and aqueous albumin (Fig. 6). In all cases, the fluorescence quantum distribution areas decrease with increasing concentration (dimer formation in water, closely spaced pair formation in methanol, multiple molecule adsorption on albumin).

The fluorescence quantum yields ϕ_F vs. concentration for the three solutions are displayed in Fig. 7. The monomer fluorescence quantum yields at low concentration are

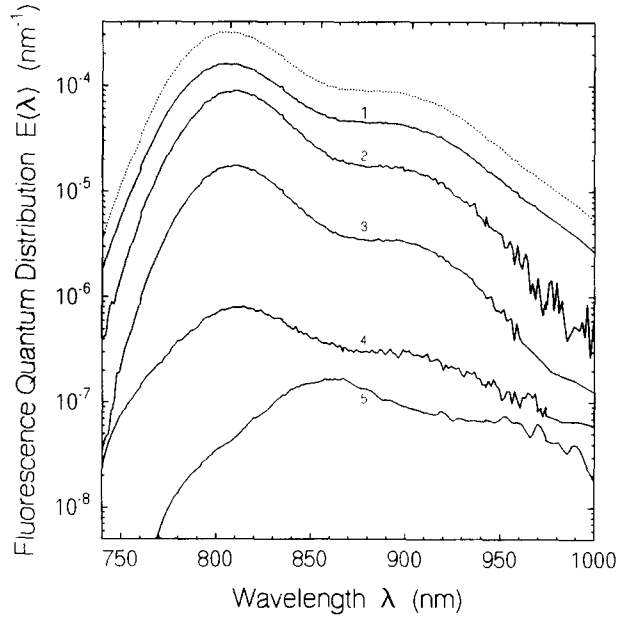

Fig. 4. Fluorescence quantum distribution $E(\lambda)$ of ICG-NaI in water at various dye concentrations (mol dm^{-3}): 1, 8.4×10^{-7}; 2, 8.4×10^{-6}; 3, 8.4×10^{-5}; 4, 8.4×10^{-4}; 5, 1.93×10^{-2}.

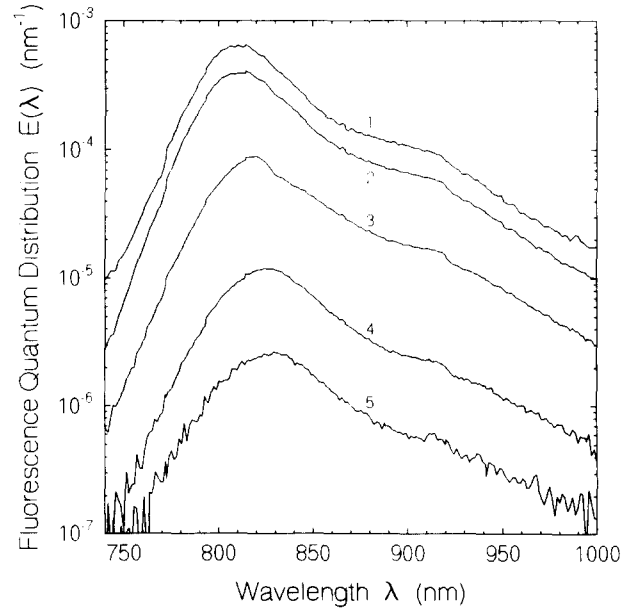

Fig. 5. Fluorescence quantum distribution of ICG-NaI in methanol at various dye concentrations (mol dm^{-3}): 1, 1.17×10^{-4}; 2, 2.35×10^{-3}; 3, 1.17×10^{-2}; 4, 4.8×10^{-2}; 5, 9.5×10^{-2}.

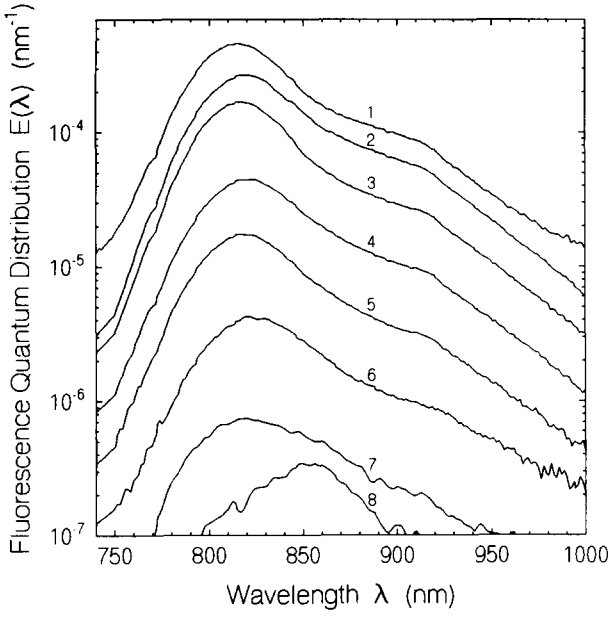

Fig. 6. Fluorescence quantum distribution of ICG-NaI in 50 g dm^{-3} aqueous albumin solution. Dye concentrations (mol dm^{-3}): 1, 1.7×10^{-5}; 2, 3.4×10^{-4}; 3, 6.9×10^{-4}; 4, 1.4×10^{-3}; 5, 2.75×10^{-3}; 6, 5.5×10^{-3}; 7, 1.1×10^{-2}; 8, 2.2×10^{-2}.

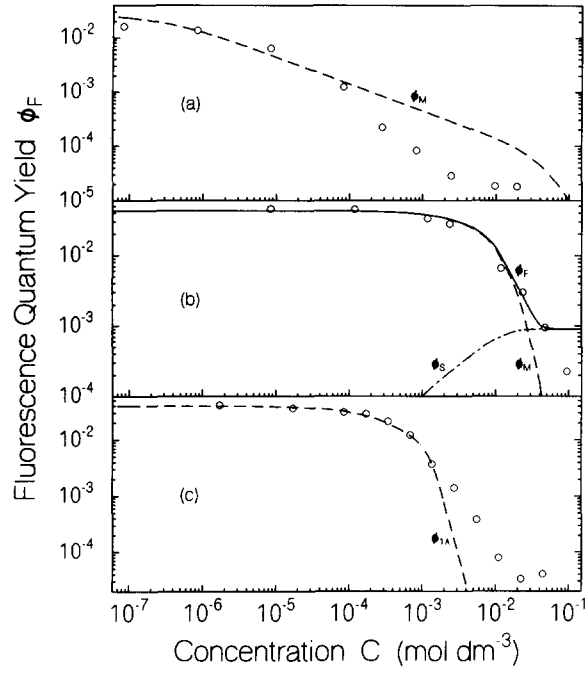

Fig. 7. Fluorescence quantum yield ϕ_F vs. concentration C for ICG-NaI in water (a), methanol (b) and 50 g dm^{-3} aqueous albumin solution (c). Open circles are experimental data; curves were calculated according to Eqs. (23)–(25).

$\phi_F(\text{water}) = 0.027 \pm 0.005$, $\phi_F(\text{albumin}) = 0.040 \pm 0.005$ and $\phi_F(\text{methanol}) = 0.043 \pm 0.005$. The low monomer fluorescence quantum yields indicate dominant non-radiative $S_1 \rightarrow S_0$ relaxation (internal conversion). Intersystem crossing studies indicate a negligibly small rate of triplet formation (quantum yield of triplet formation $\phi_T = k_{isc}\tau_F < 0.01$ [51]; k_{isc} is the intersystem crossing rate

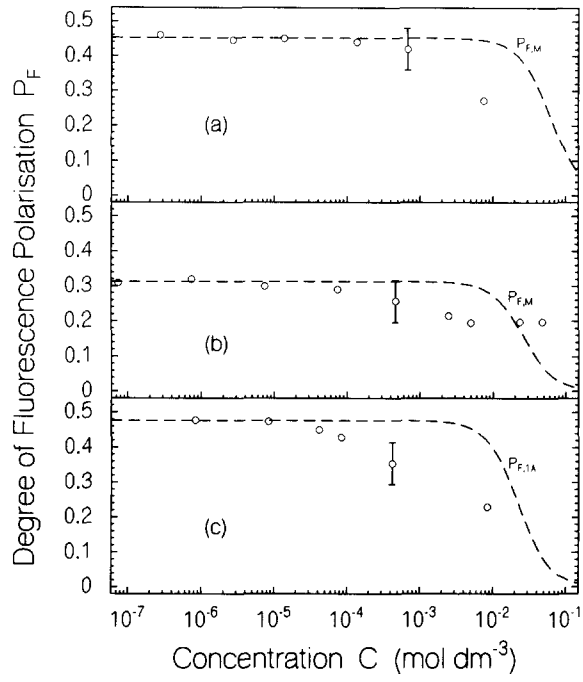

Fig. 8. Dependence of fluorescence polarization P_F on dye concentration for ICG-NaI in water (a), methanol (b) and 50 g dm^{-3} aqueous albumin solution (c). Open circles are experimental data. Broken curves are the calculated degrees of fluorescence polarization of monomers ($P_{F,M}$) and singly adsorbed molecules ($P_{F,1A}$) (Eq. (32)).

and τ_F is the fluorescence lifetime). At high concentrations, the fluorescence quantum yields become very low, indicating enhanced non-radiative decay of excited aggregates.

The degree of fluorescence polarization P_F vs. dye concentration C is plotted in Fig. 8 for the three solvents water, methanol and aqueous albumin. At low concentration, the degree of fluorescence polarization is determined by molecular reorientation within the fluorescence lifetime. At high concentration, the fluorescence polarization is reduced by energy transfer within aggregates and between excited and non-excited monomers which randomizes the transition dipole moment orientation.

4. Discussion

The concentration-dependent absorption and emission changes are discussed below in terms of dimer formation, closely spaced pair formation and dye adsorption to albumin.

4.1. Aggregation analysis

With increasing dye concentration, aggregation effects must be considered. Three systems (ICG-NaI in water, ICG-NaI in methanol and ICG-NaI in aqueous albumin) have been studied which have different aggregation behaviour. In water, ICG-NaI forms physically bound ground state dimers and oligomers. In methanol, the ICG-NaI affinity to methanol is high, reducing the probability of dimer formation. Only at

high dye concentrations does the dye–dye separation become small and (statistical) closely spaced pairs and larger aggregates are formed. In aqueous albumin solution, there is a strong affinity of ICG-NaI to albumin, leading to dye molecule adsorption on albumin.

The physically bound ground state dimer (called dimer) formation in water is described by the process

$$M + M \underset{k_{DM}}{\overset{k_{MD}}{\rightleftharpoons}} D \quad (1)$$

where M is a monomer and D is a dimer. k_{MD} and k_{DM} are the rate constants. The rate of dimer formation is given by

$$\frac{d[D]}{dt} = k_{MD}[M]^2 - k_{DM}[M] \quad (2)$$

where [D] is the dimer concentration and [M] is the monomer concentration. Under equilibrium conditions $d[D]/dt = 0$ and the dimer concentration is given by

$$D] = \frac{k_{MD}}{k_{DM}}[M]^2 = K_D[D]^2 \quad (3)$$

where K_D is the dimerization constant. In terms of mole fractions, $x_D = 2[D]/(2[D] + [M]) = 2[D]/C$ and $x_M = 1 - x_D$, where x_D is the mole fraction of molecules as dimers and x_M is the mole fraction of molecules as monomers; Eq. (3) may be solved to

$$x_D = 1 + \frac{1}{4CK_D} - \left[\left(1 + \frac{1}{4CK_D}\right)^2 - 1\right]^{1/2} \quad (4)$$

The dependence of x_D on the concentration C for various dimerization constants K_D is illustrated in Fig. 9(a). The mole fraction of molecules as dimers increases slowly with concentration. To increase x_D from 0.1 to 0.9, the dye concentration must be increased by a factor of 730. The dimerization constant K_D for the dye–water interaction is determined below (see Fig. 12(a)) by analysis of the concentration-dependent absorption spectra of ICG-NaI in water.

For ICG-NaI in methanol, dye aggregation is dominated by closely spaced pair formation. The tendency for dimer formation is weak. The dye absorption and emission are modified when dye molecules are statistically close together within an interaction volume of V_I [49,50]. The mole fraction of molecules x_S in statistically formed binary molecular centres of interaction volume V_I at a concentration C is given by [49]

$$x_S = 1 - \exp(-V_I N_A C) \quad (5)$$

where N_A is the Avogadro constant. The dependence of x_S on the concentration C for various interaction volumes V_I is illustrated in Fig. 9(b). $x_S(C)$ is much steeper than $x_D(C)$. To increase x_S from 0.1 to 0.9, the concentration must be increased by a factor of 22. For ICG-NaI in methanol, V_I is determined by analysis of the absorption cross-section spectra (Fig. 12(b), see below).

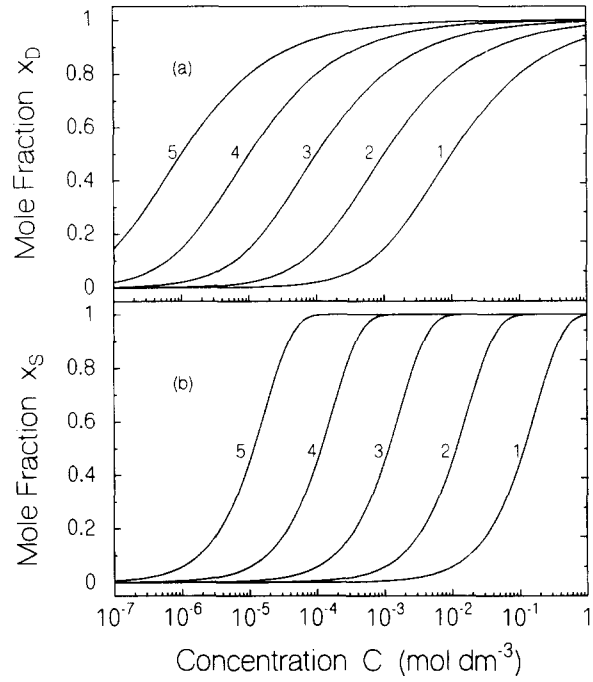

Fig. 9. (a) Theoretical dependence of mole fraction x_D of molecules as dimers vs. concentration C for various dimerization constants K_D: 1, $K_D = 10^2$ dm^3 mol^{-1}; 2, $K_D = 10^3$ dm^3 mol^{-1}; 3, $K_D = 10^4$ dm^3 mol^{-1}; 4, $K_D = 10^5$ dm^3 mol^{-1}; 5, $K_D = 10^6$ dm^3 mol^{-1}. (b) Theoretical dependence of mole fraction x_S of molecules as closely spaced pairs vs. concentration for various interaction volumes V_I: 1, $V_I = 10$ nm^3; 2, $V_I = 10^2$ nm^3; 3, $V_I = 10^3$ nm^3; 4, $V_I = 10^4$ nm^3; 5, $V_I = 10^5$ nm^3.

In aqueous albumin solution, the dye molecules are present as monomers in water (concentration $[M] = x_M C$), dimers in water (concentration $[D] = x_D C/2$), monomers adsorbed to albumin (concentration $[1A] = x_{1A} C$), two molecules adsorbed to albumin (concentration $[2A] = (x_{2A}/2)C$) and so on (concentration of n-mer $[nA] = (x_{nA}/n)C$). The distribution is governed by the processes

$$M + M \underset{k_{DM}}{\overset{k_{MD}}{\rightleftharpoons}} D \quad (6a)$$

$$M + A \underset{k_{2AM}}{\overset{k_{M1A}}{\rightleftharpoons}} 1A \quad (6b)$$

$$M + 1A \underset{k_{1AM}}{\overset{k_{M2A}}{\rightleftharpoons}} 2A \quad (6c)$$

$$M + (n-1)A \underset{k_{nAM}}{\overset{k_{MnA}}{\rightleftharpoons}} nA \quad (6d)$$

The steady state rate equation system reads

$$\frac{d[M]}{dt} = -k_{MD}[M]^2 + k_{DM}[D] - k_{M1A}[M][A] - \sum_{i=2}^{n} k_{MiA}[M][(i-1)A] + \sum_{i=1}^{n} k_{iAM}[iA] = 0 \quad (7a)$$

$$\frac{d[D]}{dt} = k_{MD}[M]^2 - k_{DM}[D] = 0 \quad (7b)$$

$$\frac{d[A]}{dt} = -k_{M1A}[M][A] + k_{1AM}[1A] \quad (7c)$$

$$\frac{d[1A]}{dt} = k_{M1A}[M][A] - k_{1AM}[1A] - k_{M2A}[M][1A] + k_{2AM}[2A] = 0 \quad (7d)$$

$$\frac{d[iA]}{dt} = k_{MiA}[M][(i-1)A] - k_{iAM}[iA] - k_{M(i+1)A}[M][iA] + k_{(i+1)A}[(i+1)A] = 0 \quad (7e)$$

$$\frac{d[nA]}{dt} = k_{MnA}[M][(n-1)A] - k_{nAM}[nA] = 0 \quad (7f)$$

with

$$[M] + 2[D] + \sum_{i=1}^{n} i[iA] = (x_M + x_D + \sum_{i=1}^{n} x_{iA})C = C \quad (8)$$

$$[A] + \sum_{i=1}^{n} [iA] = x_A C_A + C\sum_{i=1}^{n} \frac{x_{iA}}{i} = C_A \quad (9)$$

where C is the total dye concentration and C_A is the total albumin concentration.

A simple analysis of Eqs. (7a)–(7f) leads to

$$[D] = K_D[M]^2 \quad (10)$$

$$[1A] = K_{1A}[M][A] \quad (11)$$

$$[iA] = K_{iA}[M][(i-1)A] \quad \text{for } i = 2 \text{ to } n \quad (12)$$

where

$$K_{iA} = k_{MiA}/k_{iAM} \quad \text{for } i = 2 \text{ to } n$$

The solution of Eqs. (8)–(12) gives the equilibrium concentrations [M], [D], [A], [1A], ..., [nA] as a function of the equilibrium constants K_D, K_{1A}, ..., K_{nA} and the total concentrations C and C_A.

The influence of dye adsorption to albumin on the dimer formation in water is illustrated in Figs. 10 and 11. The mole fraction of dimers vs. concentration is displayed in Fig. 10 for a fixed dimerization constant of $K_D = 4.58 \times 10^5$ dm^3 mol^{-1} and varying dye adsorption constants. For curve 1, no dye adsorption takes place ($K_{1A} = 0$). Curves 2–6 are calculated for increasing dye adsorption constants of $K_{1A} = K_{2A} = K_{3A}$. In Fig. 11, the mole fractions of dye molecules as dimers (x_D) and of adsorbed dye molecules are presented. In Fig. 11(a), single molecule adsorption is considered for three different adsorption constants K_{1A}. In Fig. 11(b), single molecule and double molecule adsorption are described for $K_{1A} = K_{2A} = K_D$. The curves in Fig. 11(c) present the mole fractions up to triple molecule adsorption for

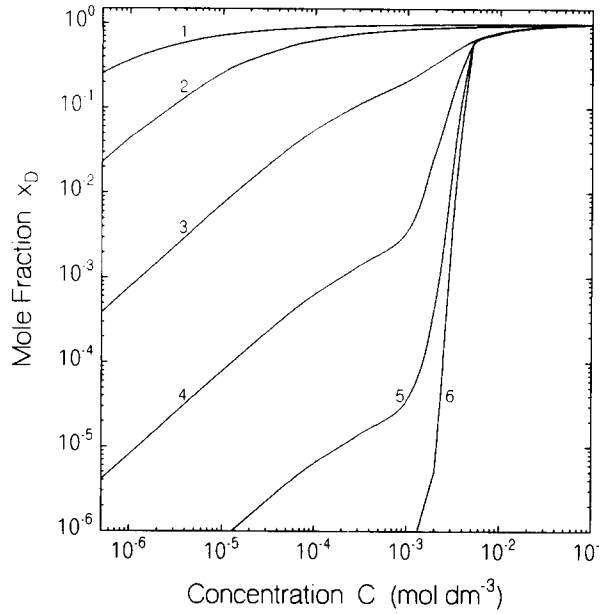

Fig. 10. Theoretical dependence of mole fraction x_D of molecules as dimers vs. dye concentration in the case of additional dye adsorption to particles. $K_D = 4.58 \times 10^5$ dm^3 mol^{-1} (from dye–water analysis). Dye adsorption stopped at $n = 3$. 1, $K_{1A} = K_{2A} = K_{3A} = 0$; 2, $K_{1A} = K_{2A} = K_{3A} = 0.01K_D$; 3, $K_{1A} = K_{2A} = K_{3A} = 0.1K_D$; 4, $K_{1A} = K_{2A} = K_{3A} = K_D$; 5, $K_{MA} = K_{DA} = K_{TA} = 10K_D$; 6, $K_{1A} = K_{2A} = K_{3A} = 100K_D$.

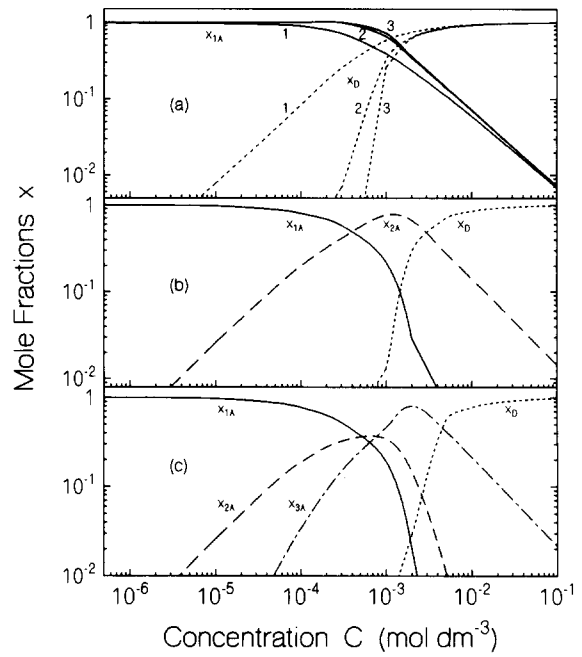

Fig. 11. Theoretical dependence of mole fraction x on dye concentration C in the case of dimerization and dye adsorption to particles. $K_D = 4.58 \times 10^5$ dm^3 mol^{-1}. (a) Mole fractions x_D and x_{1A}. Only single dye molecule adsorption is considered, i.e. $K_{2A} = 0$. 1, $K_{1A} = 0.1K_D$; 2, $K_{1A} = K_D$; 3, $K_M = 10K_D$. (b) Mole fractions x_D, x_{1A} and x_{2A}. Single molecule and double molecule adsorption is considered. $K_{1A} = K_{2A} = K_D$. (c) Mole fractions x_D, x_{1A}, x_{2A} and x_{3A}. Single, double and triple molecule adsorption is considered. $K_{1A} = K_{2A} = K_{3A} = K_D$.

$K_{1A} = K_{2A} = K_{3A} = K_D$. The number density of albumin molecules determines the adsorption capability. The dye adsorption is limited to $C = C_A$ for $K_{2A} = 0$, $C = 2C_A$ for $K_{3A} = 0$ and $C = (n-1)C_A$ for $K_{nA} = 0$ since then all adsorption sites are filled. For larger dye concentrations ($C > nC_A$ in the case of up to n molecule adsorption) a sudden increase in dimer formation in water occurs.

Some information on dye adsorption and dye dimerization in aqueous albumin will be drawn from an analysis of the concentration-dependent absorption spectra of ICG-NaI in aqueous albumin.

4.2. Absorption analysis

The concentration-dependent absorption behaviour of ICG-NaI in water up to a concentration of $C \approx 10^{-4}$ mol dm^{-3} (Fig. 1(a)) is determined by physically bound ground state dimer formation. The absorption spectrum is composed of monomer (σ_M) and dimer (σ_D) contributions according to

$$\sigma(\lambda,C) = x_M(C)\sigma_M(\lambda) + x_D(C)\sigma_D(\lambda)$$
$$= [1 - x_D(C)]\sigma_M(\lambda) + x_D(C)\sigma_D(\lambda) \quad (13)$$

with x_D given by Eq. (4). At low concentration ($C < 10^{-7}$ mol dm^{-3}), the mole fraction of molecules as dimers x_D becomes small and $\sigma(\lambda)$ approaches $\sigma_M(\lambda)$. At the two isosbestic points ($\lambda = 738$ nm and $\lambda = 828$ nm), there is $\sigma_M(\lambda) = \sigma_D(\lambda) = \sigma(\lambda)$ independent of concentration. At $\lambda_M = 780$ nm, where $\sigma_M(\lambda)$ has its maximum value, $\sigma(\lambda)$ changes strongly with concentration. The concentration dependence of $\sigma(\lambda_M)$ is used to determine K_D, $x_D(\lambda_M)$ and $\sigma_M(\lambda_M)$ by a non-linear regression fit to the experimental data [52]. The result is shown in Fig. 12(a). The fitting parameters are $K_D = 4.58 \times 10^5$ dm^3 mol^{-1}, $\sigma_D(\lambda_M) = 1.88 \times 10^{-16}$ cm^2 and $\sigma_M(\lambda_M) = 8.7 \times 10^{-16}$ cm^2.

The monomer and dimer absorption cross-section spectra are derived from two absorption cross-section spectra, $\sigma(\lambda,C_1)$ and $\sigma(\lambda,C_2)$, by solving Eq. (13) to $\sigma_M(\lambda)$ and $\sigma_D(\lambda)$. The result is

$$\sigma_M(\lambda) = \frac{x_D(C_2)\sigma(\lambda,C_1) - x_D(C_1)\sigma(\lambda,C_2)}{x_D(C_2) - x_D(C_1)} \quad (14)$$

$$\sigma_D(\lambda) = \frac{[1 - x_D(C_1)]\sigma(\lambda,C_2) - [1 - x_D(C_2)]\sigma(\lambda,C_1)}{x_D(C_2) - x_D(C_1)} \quad (15)$$

The monomer and dimer absorption cross-section spectra are shown in Fig. 1(b). The absorption cross-section spectra at $C_1 = 10^{-7}$ mol dm^{-3} and $C_2 = 8.5 \times 10^{-5}$ mol dm^{-3} of Fig. 1(a) are used in the calculations.

The concentration-dependent absorption behaviour of ICG-NaI in methanol (Fig. 2(a)) is dominated by statistical closely spaced pair formation up to about $C \approx 5 \times 10^{-2}$ mol dm^{-3} (see below). The absorption spectrum is composed of monomer (σ_M) and closely spaced pair (σ_S) contributions according to

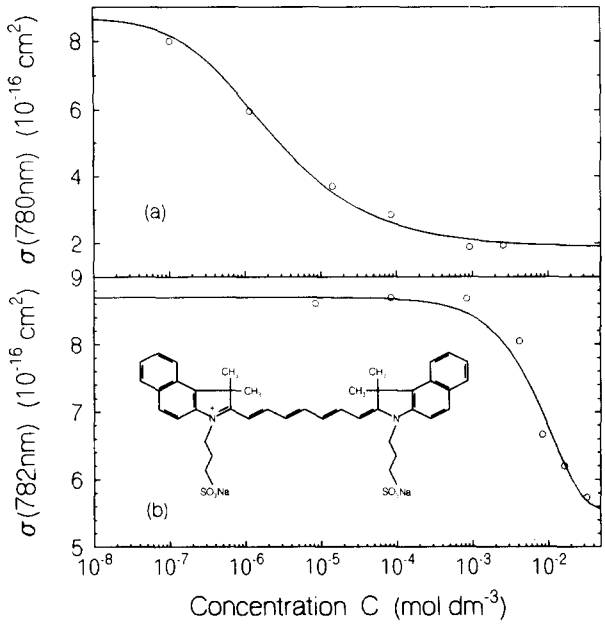

Fig. 12. (a) Absorption cross-section $\sigma(\lambda_M) = \sigma(780\text{ nm})$ of ICG-NaI in water vs. concentration. Open circles from Fig. 1. Curve is a non-linear regression fit [52] of Eqs. (4) and (13) to the experimental data (physically bound ground state dimer fit). The fitting parameters are $K_D = 4.58 \times 10^5$ dm^3 mol^{-1}, $\sigma_D(780\text{ nm}) = 1.88 \times 10^{-16}$ cm^2 and $\sigma_M(780\text{ nm}) = 8.7 \times 10^{-16}$ cm^2 ($R^2 = 0.9875$ [53]). (b) Absorption cross-section $\sigma(\lambda_M) = \sigma(782\text{ nm})$ of ICG-NaI in methanol vs. concentration. Open circles from Fig. 2. Curve is a non-linear regression fit [52] of Eqs. (5) and (16) to the experimental data (closely spaced pair fit). The fitting parameters are $V_I = 154$ nm^3 and $\sigma_S(782\text{ nm}) = 5.53 \times 10^{-16}$ cm^2 ($R^2 = 0.8662$ [53]). Structural formula of ICG-NaI is included.

$$\sigma(\lambda,C) = x_M(C)\sigma_M(\lambda) + x_S(C)\sigma_S(\lambda)$$
$$= [1 - x_S(C)]\sigma_M(\lambda) + x_S(C)\sigma_S(\lambda) \quad (16)$$

with x_S given by Eq. (5). Up to $C \approx 5 \times 10^{-4}$ mol dm^{-3}, no concentration-dependent spectral changes are observed. The full curve in Fig. 2(a) ($C = 8.4 \times 10^{-6}$ mol dm^{-3}) represents well the monomer absorption cross-section spectrum. Above $C \approx 10^{-3}$ mol dm^{-3}, the absorption at the peak monomer wavelength $\lambda_M = 782$ nm decreases because of closely spaced pair formation. Two isosbestic points are observed at $\lambda \approx 745$ nm and $\lambda \approx 813$ nm. $\sigma(\lambda_M)$ vs. concentration is displayed in Fig. 12(b). The full curve in Fig. 12(b) is a closely spaced pair non-linear regression fit (Eqs. (16) and (5)) to the experimental data (open circles). The fitting parameters are $V_I = 154$ nm^3 (diameter of interaction sphere $d_I = 6.6$ nm), $\sigma_S(782\text{ nm}) = 5.53 \times 10^{-16}$ cm^2 and $\sigma_M(782\text{ nm}) = 8.7 \times 10^{-16}$ cm^2.

The closely spaced pair absorption cross-section spectrum is derived from $\sigma_M(\lambda) \approx \sigma(\lambda, C = 8.4 \times 10^{-6}$ mol $dm^{-3})$ and $\sigma(\lambda, C = 3.3 \times 10^{-2}$ mol $dm^{-3})$ by solving Eq. (16) to $\sigma_S(\lambda)$. The resulting closely spaced pair absorption cross-section spectrum and the monomer absorption cross-section spectrum are displayed in Fig. 2(b).

The absorption behaviour of ICG-NaI in aqueous albumin solution is modified by dye adsorption to albumin. The measured absorption cross-section spectra are given by

$$\sigma(\lambda,C) = x_M\sigma_M(\lambda) + x_D\sigma_D(\lambda) + \sum_{i=1}^{n} x_{iA}\sigma_{iA}(\lambda) \qquad (17)$$

where $\sigma_{iA}(\lambda)$ is the absorption cross-section spectrum of a molecule when i molecules are adsorbed to an albumin molecule.

At low dye concentrations ($C \lesssim 10^{-5}$ mol dm^{-3}), the absorption spectra are independent of concentration. The numerical simulations (Eqs. (7)–(12) and Figs. 10 and 11) indicate that the dye molecules are predominantly adsorbed to albumin at low dye concentration (x_{1A} close to unity). Curve 1 in Fig. 3 ($C = 6.7\times10^{-6}$ mol dm^{-3}) represents $\sigma_{1A}(\lambda)$ reasonably well. The absorption peak of $\sigma_{1A}(\lambda)$ is red shifted by approximately 20 nm compared with the monomer spectrum $\sigma_M(\lambda)$ in water. The (polar) dye–albumin interaction is responsible for the shift of the absorption spectrum [54,55].

Up to $C \approx 10^{-3}$ mol dm^{-3}, no spectral shoulder is observed at the wavelength position $\lambda_D = 695$ nm of dominant dimer absorption. This indicates that dimer formation (in water surroundings) is weak up to $C \approx 10^{-3}$ mol dm^{-3}. Therefore the dye adsorption affinity coefficient K_{1A} is thought to be comparable with or larger than the dimerization equilibrium constant K_D ($K_{1A} \geqslant K_D$, see Fig. 10). The spectral changes in the concentration range 10^{-5}–2×10^{-3} mol dm^{-3} are thought to be due to multiple dye adsorption to albumin (Figs. 11(b) and 11(c)). The high concentration spectra at $C = 8.4\times10^{-3}$ mol dm^{-3} (curve 5) and $C = 1.7\times10^{-2}$ mol dm^{-3} (curve 6) resemble the high oligomer spectra observed in water and are thought to be of the same origin.

4.3. Fluorescence analysis

The fluorescence quantum distributions $E(\lambda)$ and fluorescence quantum yields ϕ_F of ICG-NaI in water, methanol and aqueous albumin are presented in Figs. 4–7. From these data, the radiative lifetimes τ_{rad} are obtained using the Strickler–Berg formula [47,56]

$$\frac{1}{\tau_{rad}} = 8\pi c_0 \frac{\int_{em} E(\lambda)\,d\lambda}{\int_{em} E(\lambda)\lambda^3 n^{-3}(\lambda)\,d\lambda} \int_{abs} \frac{\sigma_A(\lambda)}{\lambda n(\lambda)}\,d\lambda \qquad (18)$$

where c_0 is the speed of light in vacuum, $n(\lambda)$ is the refractive index of the solution at wavelength λ and $\sigma_A(\lambda)$ is the absorption cross-section distribution of the dye. The integrals extend over the $S_1 \rightarrow S_0$ fluorescence band (em) and the $S_0 \rightarrow S_1$ absorption band (abs). τ_{rad} is found to be nearly independent of concentration. For the monomers, the values obtained are τ_{rad}(ICG-NaI in water) $= 4.1 \pm 0.2$ ns, τ_{rad}(ICG-NaI in methanol) $= 4.5 \pm 0.2$ ns and τ_{rad}(ICG-NaI in aqueous albumin) $= 5.2 \pm 0.3$ ns.

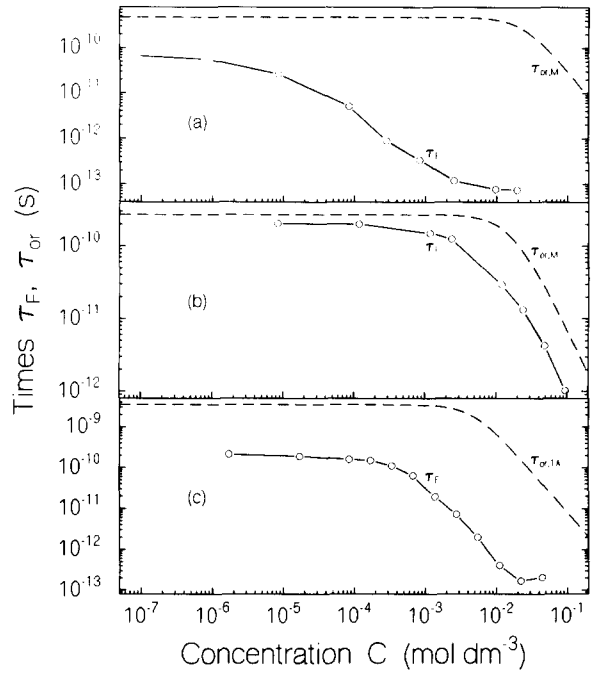

Fig. 13. Dependence of the fluorescence lifetimes τ_F (open circles and linear interpolated full curves) on dye concentration for ICG-NaI in water (a), methanol (b) and 50 g dm^{-3} aqueous albumin solution (c). Calculated reorientation times of monomers $\tau_{or,M}$ (a, b) and singly adsorbed molecules $\tau_{or,1A}$ (c) are included (Eq. (33) and Eq. (20)), broken curves).

The fluorescence lifetimes τ_F are derived from the relation

$$\tau_F = \phi_F\tau_{rad} \qquad (19)$$

In Fig. 13, τ_F is plotted vs. the dye concentration.

Dimers, oligomers, closely spaced pairs and multiple molecules adsorbed to small particles act as quenching centres of fluorescence. The fluorescence efficiency of the quenching centres is generally weak [49,50]. The monomer fluorescence is reduced in the presence of quenching centres due to energy transfer between excited and non-excited molecules towards quenching centres [49].

The electric dipole (Förster-type) energy transfer rate between excited and non-excited monomer molecules is given by

$$k_{ET} = k_F(0)\left(\frac{C}{C_0}\right)^2 = \frac{1}{\tau_F(0)}\left(\frac{C}{C_0}\right)^2 \qquad (20)$$

where $\tau_F(0) = 1/k_F(0)$ is the fluorescence lifetime at low dye concentration and C_0 is the critical transfer dye concentration. At $C = C_0$, the energy transfer rate is $k_{ET} = 1/\tau_F(0)$. C_0 is related to the critical distance of energy transfer (Förster distance) R_0 by $C_0 = (0.74N_AR_0^3)^{-1}$, and the Förster radius is obtained by the relation [49,57,58]

$$R_0^6 = \frac{3}{64\pi^5}\int_{em} E(\lambda)\sigma_{abs}(\lambda)\lambda^4 n^{-4}(\lambda)\,d\lambda \qquad (21)$$

The R_0 and C_0 data of ICG-NaI monomers in water, methanol and aqueous albumin are calculated from the monomer fluorescence quantum distributions $E_M(\lambda)$ and monomer

absorption cross-section spectra $\sigma_M(\lambda)$. The data obtained are $R_0 = 3.5$ nm and $C_0 = 5.4 \times 10^{-2}$ mol dm^{-3} for ICG-NaI in water, $R_0 = 4.9$ nm and $C_0 = 1.9 \times 10^{-2}$ mol dm^{-3} for ICG-NaI in methanol and $R_0 = 4.8$ nm and $C_0 = 2 \times 10^{-2}$ mol dm^{-3} for ICG-NaI in aqueous albumin.

The energy transfer rate k_{EQ} of excited monomers to quenching centres is given by [49,50]

$$k_{EQ} = k_{ET} x_Q = \frac{1}{\tau_F(0)} \left(\frac{C}{C_0}\right)^2 x_Q \tag{22}$$

where x_Q stands for x_D, x_S or $\sum_{i=2}^{n} x_{iA}$.

The fluorescence quantum yield $\phi_F(C)$ is composed of monomer ($\phi_M(C)$) and quenching centre ($\phi_Q(C)$) contributions according to

$$\phi_F(C) = \phi_M(C) + \phi_Q(C) \tag{23}$$

Neglecting energy backtransfer from quenching centres to monomers and assuming only one species of quenching centre, the monomer contribution $\phi_M(C)$ and quenching centre contribution $\phi_Q(C)$ are given by [59]

$$\phi_M(C) = x'_M \frac{\phi_{M,0}}{1 + x_Q g (C/C_0)^2} \tag{24}$$

and

$$\phi_Q(C) = \phi_{QM} \phi_{Q,Q} = x'_M \frac{x_Q g (C/C_0)^2}{1 + x_Q g (C/C_0)^2} \phi_{Q,0} + x'_Q \phi_{Q,0} \tag{25}$$

with

$$x'_M = \frac{x_M \sigma_M(\lambda_{pu})}{x_M \sigma_M(\lambda_{pu}) + x_Q \sigma_Q(\lambda_{pu})} \tag{26}$$

$$x'_Q = \frac{x_Q \sigma_Q(\lambda_{pu})}{x_M \sigma_M(\lambda_{pu}) + x_Q \sigma \sigma_Q(\lambda_{pu})} \tag{27}$$

λ_{pu} is the excitation light wavelength ($\lambda_{pu} = 678$ nm in our experiments). $\phi_{M,0} = \phi_F(C=0)$ is the pure fluorescence quantum yield of monomers in the absence of quenching centres. $\phi_{Q,0}$ is the pure fluorescence quantum yield of the quenching centres. $\phi_{Q,M}$ is the quenching centre fluorescence quantum yield contribution from pump-light-excited monomers and $\phi_{Q,Q}$ is the quenching centre fluorescence quantum yield contribution from pump-light-excited quenching centres. g is the ratio of the monomer → quenching centre energy transfer probability to the monomer → monomer energy transfer probability. In our calculations, we assume $g = 1$.

The fluorescence quantum distribution $E(\lambda,C)$ is composed of monomer ($E_M(\lambda,C)$) and quenching centre ($E_Q(\lambda,C)$) contributions according to

$$E(\lambda,C) = E_M(\lambda,C) + E_Q(\lambda,C) \tag{28}$$

The monomer fluorescence quantum distribution contribution is given by

$$E_M(\lambda,C) = \frac{\phi_M(C)}{\phi_{M,0}} E_{M,0}(\lambda) = \frac{x'_M}{1 + x_Q g (C/C_0)^2} E_{M,0}(\lambda) \tag{29}$$

where $E_{M,0}(\lambda) = E(\lambda, C=0)$ is the monomer fluorescence quantum distribution in the absence of quenching centres. The quenching centre contribution $E_Q(\lambda,C)$ is obtained from Eqs. (28), (29) and (25) to be

$$E_Q(\lambda,C) = E(\lambda,C) - \frac{\phi_M(C)}{\phi_{M,0}} E_{M,0}(\lambda) \tag{30a}$$

$$= \frac{\phi_Q(C)}{\phi_{Q,0}} E_{Q,0}(\lambda) = \left(x'_M \frac{x_Q g (C/C_0)^2}{1 + x_Q g (C/C_0)^2} + x'_Q \right) E_{Q,0}(\lambda) \tag{30b}$$

where $E_{Q,0}(\lambda)$ is the quenching centre fluorescence quantum distribution.

The system ICG-NaI in water is characterized by the presence of monomers, dimers and oligomers. The broken curve in Fig. 7(a) shows the expected monomer fluorescence (Eq. (24)). The fitting parameters are $\phi_{M,0} = 0.027$, $K_D = 4.58 \times 10^5$ dm^3 mol^{-1} (see Fig. 12(a)) and $C_0 = 5.4 \times 10^{-2}$ mol dm^{-3} (Eq. (21)). Up to $C \approx C_0$, the monomer fluorescence contribution ϕ_M is determined by the mole fraction of monomers $x_M = 1 - x_D$ (Fig. 12(a)). The fit to the experimental data is good up to $C \approx 10^{-4}$ mol dm^{-3}. At higher concentrations, the total fluorescence quantum yield ϕ_F is less than the calculated monomer fluorescence quantum yield and the fluorescence behaviour cannot be described by a simple monomer–dimer equilibrium. The formation of larger aggregates reduces the monomer concentration below the monomer–dimer equilibrium and causes a decrease in the fluorescence quantum yield.

The monomer fluorescence quantum distribution $E_{M,0}(\lambda)$ is shown by the dotted curve in Fig. 4. It is obtained from the fluorescence quantum distribution $E(\lambda, C = 8.4 \times 10^{-7}$ mol dm$^{-3})$ by the relation $E_{M,0}(\lambda) = E(\lambda, C = 8.4 \times 10^{-7}$ mol dm$^{-3}) \phi_{M,0} / \phi(C = 8.4 \times 10^{-7}$ mol dm$^{-3})$ (at this concentration $E(\lambda,C) = E_M(\lambda,C)$ and $\phi_F(C) = \phi_M(C) \approx 0.5 \phi_{M,0}$).

The solution ICG-NaI in methanol is well characterized by the presence of monomers and closely spaced pairs up to $C \approx 5 \times 10^{-2}$ mol dm^{-3}. The full curve in Fig. 7(b) shows the fit of Eq. (23) to the experimental data. The fitting parameters are $\phi_{M,0} = 0.043$, $V_I = 154$ nm^3 (Fig. 12(b)), $C_0 = 1.9 \times 10^{-2}$ mol dm^{-3} (Eq. (21)) and $\phi_{Q,0} = \phi_{S,0} = 9 \times 10^{-4}$. In Fig. 7(b), the broken curve shows $\phi_M(C)$ and the broken-dotted curve shows $\phi_S(C)$. Up to $C \approx 2.5 \times 10^{-2}$ mol dm^{-3}, the monomer fluorescence dominates. For the experimental point at $C = 4.8 \times 10^{-2}$ mol dm^{-3}, the closely spaced pair fluorescence dominates. At $C = 9.5 \times 10^{-2}$ mol dm^{-3}, the fluorescence is reduced by

larger aggregates. It should be noted that, at this concentration, on average, 12 molecules are within the interaction volume of $V_I = 154$ nm^3. In Fig. 5, curve 1 represents the monomer fluorescence quantum distribution ($E_{M,0}(\lambda)$), curve 4 represents the closely spaced pair fluorescence quantum distribution ($E_{S,0}(\lambda)$) and curve 5 is caused by larger closely spaced aggregates.

For ICG-NaI in 50 g dm^{-3} aqueous albumin solution, the fluorescence is dominated by emission from single adsorbed molecules up to $C = 2\times10^{-3}$ mol dm^{-3}. The broken curve in Fig. 7 shows $x_{1A}(C)\phi_{1A,0}$, which is practically identical to $\phi_{1A}(C)$ in the presented concentration region of the curve ($C \ll C_0 = 2\times10^{-2}$ mol dm^{-3}). In the region of 2×10^{-3} mol dm$^{-3} \lesssim C \lesssim 8\times10^{-3}$ mol dm^{-3}, the fluorescence seems to be dominated by double and triple adsorbed dye molecules. Above $C \approx 8\times10^{-3}$ mol dm^{-3}, oligomers in water seem to be responsible for the fluorescence. In this region, the fluorescence quantum yield becomes comparable with the situation of the dye in pure water. Curve 1 in Fig. 6 is practically identical to the fluorescence quantum distribution $E_{1A,0}(\lambda)$ of single adsorbed molecules to albumin ($E_F(\lambda, C = 1.7\times10^{-5}$ mol dm$^{-3}) \approx E_{1A,0}(\lambda)$). Curve 6 is thought to be the fluorescence quantum distribution of double and triple adsorbed dye molecules. Curve 8 is due to oligomers in water. The shape of curve 8 is similar to the shape of curve 5 in Fig. 4, representing the oligomer fluorescence quantum distribution in water.

The stimulated emission cross-section spectra are derived from the fluorescence quantum distributions $E(\lambda)$ and the radiative lifetime τ_{rad} (Eq. (18)) by the relation [60]

$$\sigma_{em}(\lambda) = \frac{\lambda^4}{8\pi n^2(\lambda) c_0 \tau_{rad}} \frac{E_F(\lambda)}{\int_{em} E_F(\lambda) E_F(\lambda') d\lambda'} \quad (31)$$

The calculated stimulated emission cross-section spectra of the monomers in water (a) and methanol (b) and of the singly adsorbed molecules on albumin (c) are displayed in Fig. 14.

The degree of fluorescence polarization P_F depends on the reorientation time τ_{or} of the S_0–S_1 transition dipole moment due to molecular reorientation ($\tau_{or,m}$) and energy transfer (k_{ET}) according to the relation [48,61,62]

$$\frac{1}{P_F} - \frac{1}{3} = \left(\frac{1}{P_{F,0}} - \frac{1}{3}\right)\left(1 + \frac{\tau'_F}{\tau_{or}}\right) \quad (32)$$

where $P_{F,0}$ is the fluorescence polarization in the case of $\tau_{or} = \infty$ and τ'_F is the fluorescence lifetime of the emitting species. For the excitation of isotropic dye solutions with linearly polarized light, a value of $P_{F,0} = 0.5$ is obtained if the transition dipole moments of absorption and emission are parallel to one another [46,48]. The transition dipole reorientation time is approximately given by [62]

$$\frac{1}{\tau_{or}} = \frac{1}{\tau_{or,m}} + k_{ET} \quad (33)$$

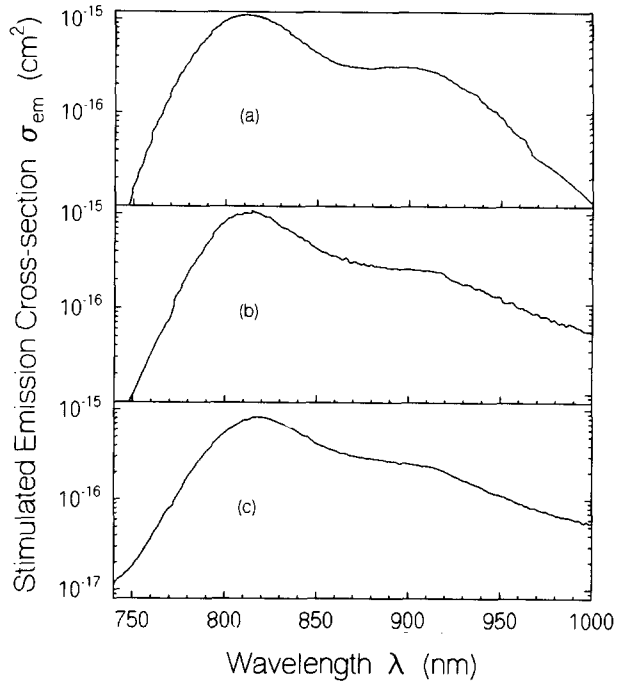

Fig. 14. Stimulated emission cross-sections for: (a) ICG-NaI monomers in water; (b) ICG-NaI monomers in methanol; (c) single ICG-NaI molecules adsorbed to albumin in water.

At low concentrations, τ_{or} is equal to the molecular reorientation time $\tau_{or,m}$.

For the reference dye solution HITCI in methanol, we obtain $P_F \approx 0.16$ using $\tau_{or} \approx 200$ ps [63] and $\tau_F \approx 500$ ps [45]. Using the experimental P_F data at low concentration (Fig. 8), Eq. (32) gives $\tau_{or,m}$(water) $= 480 \pm 150$ ps, $\tau_{or,m}$(methanol) $= 270 \pm 100$ ps and $\tau_{or,m}$(albumin) $= 3.5 \pm 2$ ns. For methanol and water, the molecular reorientation time is roughly proportional to the dynamic viscosity η (η(water) $= 10^{-3}$ Pa s; η(methanol) $= 5.9\times10^{-4}$ Pa s). The adsorption of the dye molecules to albumin increases the reorientation time.

The concentration-dependent total reorientation times of monomers ($\tau_{or,M}$) and singly adsorbed molecules ($\tau_{or,1A}$) can be calculated using Eqs. (33) and (20). The resulting curves are included in Fig. 13. The degree of fluorescence polarization of monomers and singly adsorbed molecules is calculated using Eq. (32) and $\tau'_F = \tau_F(0)$. The curves obtained are included in Fig. 8. In water, the experimental fluorescence polarization decreases with the onset of higher oligomer formation (Fig. 7(a)). In methanol, the experimental fluorescence polarization decreases slightly with increasing concentration. In the case of dye adsorption to albumin, the measured fluorescence polarization decreases with the onset of double molecule adsorption.

5. Conclusions

The concentration-dependent absorption and emission behaviour of ICG-NaI in water, methanol and aqueous

albumin solution was studied experimentally and theoretically. The aggregation of the dye in the three solvents was different. In water, physically bound ground state dimer formation occurred at low dye concentrations and strong higher oligomer formation started at moderate dye concentrations. In methanol, the tendency for bound ground state dimer formation was weak. At high dye concentrations, the absorption and emission spectra were modified by near-neighbour dye–dye interactions (closely spaced pairs and closely spaced multiple molecules). In aqueous albumin solutions, dye adsorption occurred to the nanometre-sized macromolecular albumin particles. Dye adsorption dominated over dimerization and oligomer formation as long as the dye number density was less than a few times the nanometre particle number density.

The adsorption of two or more molecules to a single albumin particle led to the formation of artificial dye clusters. The presented analysis of the adsorption of ICG on albumin should apply quite generally to the adsorption of small- and medium- sized molecules to micro- and meso-sized particles [41].

The observed spectroscopic parameters of ICG-NaI indicate that the dye should be a promising fast saturable absorber [64] (especially ICG-NaI in water because of the short τ_F) and a promising picosecond-pulse-pumped laser dye [65] (especially ICG-NaI in methanol because of the high stimulated emission cross-section) in the near-IR spectral region.

References

[1] I.J. Fox, I.G.S. Brooker, D.W. Heseltine, H.E. Essex and E.H. Wood, *Am. J. Physiol., 187* (1956) 599.
[2] I.J. Fox and E.H. Wood, *Mayo Clin. Proc., 35* (1960) 732.
[3] T. Nahimisa, *Tokai J. Exp. Clin. Med., 7* (1982) 419.
[4] F.J. Klocke, D.G. Greene and R.C. Koberstein, *Circulation Res., 22* (1968) 841.
[5] H. Schad, H. Brechtelsbauer and K. Kramer, *Pfluegers Arch., 370* (1977) 139.
[6] K. Haneda and T. Horiuchi, *Tohoku J. Exp. Med., 148* (1986) 49.
[7] E.C. Bradley and J.W. Berr, *Life Sci., 7* (1968) 1001.
[8] C.M. Leevy, C.B. Leevy and M.M. Howard, in C. Davidson (ed.), *Problems in Liver Diseases*, Thieme, Stuttgart, New York, 1979, p. 42.
[9] M.W. Gottlieb, H.H. Stratton, J.C. Newell and D.M. Shah, *Arch. Surg., 119* (1984) 264.
[10] G. Paumgartner, P. Probst, R. Kraines and C.M. Leevy, *New York Acad. Sci., 170* (1970) 134.
[11] J. Aubrecht and F. Perlik, *Cesk. Farm., 39* (1990) 155.
[12] J.C. Fleishaker, H. Friedman and S.R. Pollock, *Pharm. Res., 8* (1991) 162.
[13] L.A. Bauer, K. Murray, J.R. Horn, K. Opheim and J. Olsen, *Eur. J. Clin. Pharmacol., 37* (1989) 257.
[14] S. Takaya, S. Icoatsuki, T. Noguchi, H. Hisaaki, I. Zaghloul, R. Venkataraman and T.E. Starzl, *Jpn. J. Surg., 19* (1989) 49.
[15] A. Craandijk and C.A. Van Beek, *Bnt. J. Ophthal., 60* (1976) 377.
[16] R.W. Flower and B.F. Hochheimer, *The Johns Hopkins Medical Journal, 138* (1976) 33.
[17] R.C. Benson and H.A. Kues, *Phys. Med. Biol., 23* (1978) 159.
[18] B. Chance, K. Kang, L. He, J. Weng and E. Sevick, *Proc. Natl. Acad. Sci. USA, 90* (1993) 2423.
[19] J.N. Ketley, W.H. Habig and W.B. Jakoby, *J. Biol. Chem., 250* (1975) 8670.
[20] K. Sauda, T. Imasaka and N. Ishibashi, *Anal. Chem., 58* (1986) 2649.
[21] G. Timberlake, A. Patmore, A. Shallal, D. McHugh and J. Marshall, *SPIE, 1882* (1993) 244.
[22] S.D. Decoste, W. Farinelli, T. Flotte and R.R. Anderson, *Laser Surg. Med., 12* (1992) 25.
[23] S.K. Libutti, M.C. Oz, R.S. Chuk, J.S. Anteri, H. Hibshoosh, R. Nowygrod and M.R. Treat, *SPIE, 1200* (1990) 172.
[24] Y. Gu, J.-H. Li and Z.-H. Gou, *SPIE, 1616* (1991) 266.
[25] D.D. Michie, R.S. Goldsmith and A.D. Mason, Jr., *Exp. Biol. Med., 111* (1962) 111.
[26] K.J. Baker, *Proc. Soc. Exp. Biol. Med., 122* (1966) 957.
[27] W.F. Sutterer, I.E. Hardin, R.W. Benson, L.J. Krovetz and G.L. Schiebler, *Am. Heart J., 72* (1969) 373.
[28] K.B. Saunders, J.I.E. Hoffman, M.I.M. Noble and R.J. Domenech, *J. Appl. Physiol., 28* (1970) 190.
[29] J. Gathje, R.R. Stauer and K.R.N. Nicholes, *J. Appl. Physiol., 29* (1970) 181.
[30] R. Simmons and R.J. Shephard, *J. Appl. Physiol., 30* (1971) 502.
[31] M.R. Tripp, G.M. Cohen, D.A. Gerasch and I.J. Fox, *Proc. Soc. Exp. Biol. Med., 143* (1973) 880.
[32] V.M.J. Owen, *Clin. Biochem., 6* (1973) 132.
[33] M.L.J. Landsman, G. Kwant, G.A. Mook and W.G. Zijlstra, *J. Appl. Physiol., 40* (1976) 575.
[34] G. Scheibe, *Angew. Chem., 50* (1937) 51.
[35] E.E. Jelly, *Nature, 138* (1936) 1009.
[36] T. Imasaka, T. Okazaki and N. Ishibashi, *Anal. Chim. Acta, 208* (1988) 325.
[37] G. Patonay, M.D. Antoine and A.E. Boyer, *SPIE, 1435* (1991) 52.
[38] T. Imasaka, H. Nakagawa, T. Hiroyuki and N. Ishibashi, *Anal. Chem., 62* (1990) 2404.
[39] *Data Sheet ICG-Pulsion*, Pulsion Medizintechnik, Kirchenstrasse 88, D-81675 München, March, 1994.
[40] T. Peters, in C.B. Anfinsen, J.T. Edsall and F.M. Richards (eds.), *Advances in Protein Chemistry*, Vol. 37, Academic Press, New York, 1985, p. 161.
[41] S. Lowell and J.E. Shields, *Powder Surface Area and Porosity*, Chapman & Hall, London, 3rd edn., 1991.
[42] A. Penzkofer and W. Leupacher, *J. Lumin., 37* (1987) 61.
[43] W. Bäumler and A. Penzkofer, *Chem. Phys., 140* (1990) 75.
[44] U. Brackmann, *Lambdachrome Laser Dyes, Data Sheets*, Lambda-Physik, Göttingen, 1994.
[45] P. Sperber, W. Spangler, B. Meier and A. Penzkofer, *Opt. Quant. Electron., 20* (1988) 395.
[46] R. Lakowicz, *Principles of Fluorescence Spectroscopy*, Plenum, New York, 1983.
[47] S.J. Strickler and R.A. Berg, *J. Chem. Phys., 37* (1962) 814.
[48] C.A. Parker, *Photoluminescence of Solutions*, Elsevier, Amsterdam, 1968.
[49] Th. Förster, *Fluoreszenz Organischer Verbindungen*, Vandenhoeck and Ruprecht, Göttingen, 1951.
[50] Y. Lu and A. Penzkofer, *Chem. Phys., 107* (1986) 175.
[51] S. Reindl and A. Penzkofer, to be published.
[52] J.A. Nelder and R. Mead, *Comput. J., 7* (1965) 308.
[53] R.R. Sokal and F.J. Rohlf, *Biometry*, W.H. Freeman, New York, 2nd edn., 1981, p. 631.
[54] M. Magata and T. Kubota, *Molecular Interaction and Electronic Spectra*, Dekker, New York, 1970, Chapter 8, p. 371 ff.
[55] A.V. Deshpande, A. Beidoun, A. Penzkofer and G. Wagenblast, *Chem. Phys., 148* (1990) 141.
[56] J.B. Birks and D.J. Dyson, *Proc. R. Soc. London, Ser. A, 275* (1963) 135.
[57] Th. Förster, in O. Sinanoglu (ed.), *Modern Quantum Chemistry*, Part III, Academic Press, New York, 1986.

[58] G.R. Fleming, *Chemical Applications of Ultrafast Spectroscopy*, Oxford University Press, New York, 1985, p. 93.
[59] M. Wittmann and A. Penzkofer, *Chem. Phys., 172* (1993) 339.
[60] O.G. Peterson, J.P. Webb, W.C. McColgin and J.H. Eberly, *J. Appl. Phys., 42* (1971) 1917.
[61] P. Weidner and A. Penzkofer, *Chem. Phys., 191* (1995) 303.
[62] G. Weber, in D.M. Hercules (ed.), *Fluorescence and Phosphorescence Analysis, Principles and Applications*, Interscience Publishers, New York, 1966, p. 217.
[63] G.S. Beddard, T. Doust and G. Porter, *Chem. Phys., 61* (1981) 17.
[64] A. Penzkofer, *Appl. Phys. B, 46* (1988) 43.
[65] A. Seilmeier, B. Kopainsky and W. Kaiser, *Appl. Phys., 22* (1980) 359.